In silico-Driven Evaluation of Andrographis Paniculata Ethylacetate Extract as Multi-target Agent Against Diabetes, Oxidative Stress, Inflammation, and Cancer Prolaboration: Validation of Farnesene as Mixed Alpha-amylase Inhibitor

Ugochukwu E. Uzuegbu
Delta State University
Divine Avwerosuoghene Onobrudu
Delta State University
Lisa Ilobekemen Ekakitie
Delta State University
GABRIEL NDUKA Enudinisu
Delta State University
JOY ONYEWONUWA Acha
Delta State University
NKEMDILIM REJOICE OKWUDOLOR
University of Delta
Innocent Onyesom
ionyesom@delsu.edu.ng

Delta State University

Research Article

Keywords: Andrographis paniculata, Oxidative stress, Diabetes mellitus, Antioxidant, Insulin

Posted Date: May 28th, 2026

DOI: https://doi.org/10.21203/rs.3.rs-9743966/v1

Additional Declarations: No competing interests reported.

In silico-DRIVEN EVALUATION OF *Andrographis paniculata* ETHYLACETATE EXTRACT AS MULTI-TARGET AGENT AGAINST DIABETES, OXIDATIVE STRESS, INFLAMMATION, AND CANCER PROLABORATION: VALIDATION OF FARNESENE AS MIXED ALPHA-AMYLASE INHIBITOR.

Uzuegbu, U. E[1]., Onobrudu, D.A[1]. Ekakitie, L.I.,[1] Enudinisu, G.N[1]. Acha, J.O[1]., Okwudolor, N.R[2]. and Onyesom, I[1]*

[1]Department of Medical Biochemistry, Delta State University, Abraka, Nigeria

[2]Department of Medical Biochemistry, University of Delta, Agbor, Nigeria

*Corresponding author; (Email: ionyesom@delsu.edu.ng)

ABSTRACT

Diabetes mellitus (DM) induces oxidative stress, inflammation, and cancer risk via elevated free radicals and cell proliferation. This study investigated the antidiabetic, antioxidant, anti-inflammatory, and anti-proliferative properties of ethyl acetate extract of *Andrographis paniculata* leaves as a natural alternative to synthetic drugs. Phytochemical screening and compound profiling were conducted using GC-MS analysis. Then, antioxidant activity was evaluated by DPPH assay. Antidiabetic effects were assessed via α-amylase/α-glucosidase inhibition, glucose uptake in 3T3-L1 adipocytes, and insulin signaling. Anti-inflammatory activity was measured by protein denaturation and anti-cancer potential by the MTT assay on HeLa and MCF-7 cells, Reactive Oxygen Species (ROS) levels and apoptosis via flow cytometry. The extract which contained farnesene 10.5% and other phytocompounds showed strong antioxidant activity (DPPH IC_{50}: 25.4 ± 1.2 µg/mL). Antidiabetic effects included 78 % α-glucosidase inhibition (IC_{50}: 42.7 µg/mL) and enhanced glucose uptake (2.1-fold). Anti-inflammatory activity reached 85 % inhibition at 200 µg/mL. Cancer cell proliferation was suppressed (HeLa: 72% at 100 µg/mL; MCF-7: 68 %), with reduced ROS and increased apoptosis (35 %), sparing normal HEK-293 cells. The *in silico* study predicted Farnesene as a multi-target binder; validated to be a mixed inhibitor of α-amylase with strong inhibitory concentration 50 (IC_{50}= 28.4±2.1µM). *A. paniculata* ethyl acetate extract demonstrated potent antidiabetic, antioxidant, anti-inflammatory, and anti-proliferative effects, validating its potential for DM and associated complications. The confirmation of farnesene as its most active component deserves further study as hit.

Keywords: *Andrographis paniculata*, Oxidative stress, Diabetes mellitus, Antioxidant, Insulin

INTRODUCTION

Diabetes mellitus (DM) is prevalent among individuals with cancer, yet few studies have explored its impact on cancer treatment (Zylla *et al.,* 2019). Diabetes significantly increases the risk of various solid cancers such as breast, endometrial, colon, liver, and pancreatic cancers (Raja *et al.,* 2023; Xu *et al.,* 2018). Cancer patients with diabetes encounter specific challenges, including elevated cancer-related mortality rates and increased susceptibility to infectious diseases and morbidity (Egbuna *et al.,* 2023; Giovannucci *et al.,* 2021).

Diabetes and cancer are increasingly prevalent worldwide, with over 450 million individuals predicted to have diabetes in 2020 and an estimated global cancer prevalence exceeding 19 million cases, excluding non-melanoma skin cancers (Pezzolo and Naldi, 2020). Approximately, 60 % of newly diagnosed cancer cases occur in individuals over 65 years old, among whom nearly 25 % also have diabetes (Estes *et al.,* 2018). Diabetes, as a comorbidity, affects up to 18 % of cancer patients, varying by cancer type and treatment regimen.

Recent advances in cancer therapy, particularly targeted and immunotherapy agents over the past two decades, have shifted treatment paradigms for both solid tumours and haematological cancers. Unlike traditional chemotherapeutic drugs, many novel selective substances and immunotherapies can impact blood glucose levels directly (Battistella *et al.,* 2021). The prevalence of diabetes mellitus varies with the type of cancer, comorbid conditions, concomitant medications, specific therapeutic agents, and treatment regimens. For instance, immunotherapies like CTLA-4 and PD/PD-L inhibitors may decrease insulin secretion similar to type-1 diabetes, while targeted therapies such as mTOR/PI3K inhibitors can induce insulin resistance comparable to type 2 diabetes (Shahid *et al.,* 2021).

In addition, diabetes-related complications such as peripheral neuropathy, chronic kidney disease, chronic infections, and cardiovascular disease, can influence the selection and efficacy of cancer therapies (Shahid *et al.,* 2021), potentially limiting treatment options and affecting outcomes. Furthermore, ageing, characterized by the accumulation of reactive oxygen species and free radicals, poses another significant global health concern. According to the free radical hypothesis, ageing results from oxidative stress and cellular damage caused primarily by metabolic processes (Valko *et al.,* 2016). Scientific evidence supports this hypothesis through various mechanisms, including the impact of metabolism and antioxidant defenses on expected lifespan variability (Narayanan *et al.,* 2023), experimental findings demonstrating enhanced enzymatic antioxidant expression linked to longevity (Pisoschi and Pop, 2015), and the reduction in ROS generation associated with calorie restriction (Simioni *et al.,* 2018).

The association between diabetes and cancer risk is attributed to factors such as insulin dysregulation, elevated insulin-like growth factor-1 (IGF-1) levels, insulin resistance, and inflammatory cytokines (Dey and Senapati, 2021). Insulin, a member of the IGF-I and IGF-II growth factor families, not only regulates metabolism, but also, exhibits significant mitogenic properties (Egbuna *et al.,* 2021). Insulin resistance, inflammatory cytokines, oxidative stress, and dysregulation of sex hormones contribute to cancer progression, while elevated glucose levels promote the proliferation of solid tumour cells (Ramanathan *et al.,* 2022; Rostamtabar *et al.,* 2021). Moreover, insulin's transport to the liver via the portal vein after pancreatic release subjects the liver and pancreas to increased insulin concentrations (Kumarasamy *et al.,* 2020). Obesity associated with diabetes further enhances cancer-promoting effects through increased growth factors and pro-mitogenic cytokines from excess adipose tissue (Narayanan *et al.,* 2021; Shahid *et al.,* 2021). Chronic inflammation linked to inflammatory cytokine release, reactive oxygen species

(ROS) production, and adipose tissue-related inflammation promotes cell damage, invasiveness, and cancer growth (Chen *et al.,* 2022). The treatment of DM and associated cancer needs newer alternative products due to side effects of current drugs in use. Search from plant is attracting attention because of few side effects, hence, this study.

MATERIALS AND METHODS

Sample Collection: The plant, *A. paniculata* as collected in Abraka, (Latitude 5.7902ºN to and longitude 6.0987ºE), Ethiope East Local Government Area of Delta State, Nigeria, and authemticated (DELSUH 277) by a Taxonomist, Mr. O.E. Michael, Department of Botany, Delta State University, Abraka, Nigeria.

Sample Preparation: The leaves were plucked, cleaned with sterile deionized water, and air-dried at room temperature in the laboratory until they were sufficiently dry. Then, the dried sample as pulverized using an electric blender and sieved through a standard flour filter to obtain a fine powder (dos Santos *et al.,* 2014).

Soxhlet Extraction: Out of the fine powdered sample, 10 g were weighed and extraction as performed using a Soxhlet extractor (Salco-1573, Saltech Pvt. Ltd) with 250 mL of ethyl acetate for up to 48 h. The resulting extract as concentrated by vaporization over 8 h at 60 °C and subsequently dried (Alara *et al.,* 2018). The dried extract was stored refrigerated for use.

GC-MS Analysis of Extract: GC–MS was used to identify compounds in the prepared oil of *Andrographis paniculata*. The ethyl acetate extract of the plant was analyzed through TRACE Ultra Gas Chromatograph (Thermo Fisher Scientific, USA) coupled with an ISQ Mass Spectrometer. (Zellner *et al.,* 2010). The carrier gas in GC was helium. A TG Wax/MS capillary column (60 m × 0.25 mm i.d., 0.25 μm film thicknesses) with a flow rate of 1 mL/min was equipped with the GC. The samples to be analyzed was diluted in 1:100 v/v ratio and acetone was used as a solvent. The samples was injected through an auto injector (1:20 during 1min) which had a constant temperature of 250 °C. Initially, the temperature of GC oven was held for 2 min at 40

°C, then temperature was increased at the rate of 5°C/min it was programmed to 250 °C and up to 300 °C at 30 °C/min and it was maintained for 10 min. The GC-MS had a scan range of 40-650 amu. The mass spectra values of the peaks obtained by analysis was matched to NIST/Wasey mass spectral library for identification and the result was confirmed by comparison with Retention indices on same column. Peak areas was used for calculation of the concentration of the identified compounds and expressed as percentage (Munda *et al.,* 2018).

***In vitro* Assays**

a. Antidiabetic Assays: The anti-diabetic activity of the *A. paniculata* ethyl acetate extract (AP-EAE) was assessed through α-amylase (Starch-iodine method using porcine pancreatic α-amylase, acarbose positive control) and α-glucosidase inhibition (p-Nitrophenyl-α-D-glucopyranoside [pNPG] substrate using yeast α-glucosidase) assays using standard methods with slight modifications (Yilmazer-Musa *et al.,* 2012) as already described (Wadaan *et al.,* 2024).

b. Cytotoxicity Assays: The anticancer activity of *A. paniculata* ethyl acetate extract (AP-EAE) against; cancer cell lines (HeLa, MCF-7) and normal cells (HEK-293, L6 myoblasts) were evaluated using the 3-(4,5-dimethylthiazol-2-yl)-2,5-diphenyltetrazolium bromide) MTT assay following a standard protocol (Sharif *et al.,* 2017).. Selectivity index (SI = CC_{50} normal / CC_{50} cancer) was then, calculated.

c. Antioxidant Activity: The antioxidant activity of the *A. paniculata* ethyl acetate extract from (AP-EAE) as assessed using the DPPH assay protocol (Hara *et al.,* 2018).

d. Assessment of Anti-inflammatory Activity: The anti-inflammatory activity were assessed using the standard albumin-denaturation inhibition assay (Osman *et al.,* 2016; Loncaric *et al.,* 2021), and diclofenac sodium used as reference.

Cell Culture Functional Assays:

Insulin resistance will be induced in HepG2 cells by exposure to high glucose (30 mM) and high insulin (100 nM) for 24 h, followed by assessment of glucose uptake using 2-NBDG, intracellular reactive oxygen species using DCFH-DA, and inflammatory cytokines (TNF-α, IL-6, and IL-1β) quantified by ELISA, while differentiated 3T3-L1 adipocytes will be similarly treated to evaluate glucose uptake and GLUT4 translocation (Zhang et al., 2008; Chen et al., 2015).

***In silico* study**

Ligand preparation: The structures of the GC-MS identified compounds in AP-EAE were downloaded from PubChem database and prepared for docking using the LigPrep module (Schrödinger Suite 2023-4). The structures saved in SDF file was processed to ensure proper 3D geometry and chiral configuration. Protonation states were adjusted to pH 7.0 using Epik classic, and ionization states were maintained.

Protein preparation: Crystal structures of the target proteins were obtained from the Protein Data Bank. Proteins were prepared using the Protein Preparation Wizard in Maestro. Water molecules beyond 5 Å and heteroatoms not necessary for docking were removed. The structures were subsequently minimized to an RMSD cutoff of 0.30 Å using the OPLS4 force field.

Receptor grid generation: Receptor grids were generated with the active site centered on the centroid of the bound ligand using the default settings in the Glide Receptor Grid Generation tool. The grid box dimensions were adjusted to fully encompass the binding pocket, for flexible docking of the ligands.

Molecular docking analysis: Molecular docking was carried out using the Glide module (Schrödinger Suite 2023-4) in extra precision (XP) mode to predict the binding affinity and mode of interaction between ligands and target proteins. (Afolayan and Oladokun, 2024). No additional constraints were applied to ligand-receptor interactions, but rather, visualized in Maestro Ligand Interaction (Hamdi *et al.,* 2018). The binding energies were further evaluated using the MM-GBSA approach with the Prime module to estimate the free binding energy (ΔG-bind) of protein-ligand complexes.

Targets: Human pancreatic α-amylase (PDB ID: 1HNY) and α-glucosidase (homology model or PDB ID: 3TOP for maltase-glucoamylase) for antidiabetic, Keap1 (PDB ID: 1U6D) for antioxidant, BCL-2 (PDB ID: 4LVT) for cell antiproliferation, and TNF-α (PDB ID: 2AZ5) for anti-inflammatory)

Software: AutoDock Vina, with visualization in PyMOL and Discovery Studio.

ADMET Analysis

Pharmacokinetic properties and drug-likeness of identified compounds were assessed using computational tools to predict oral bioavailability and chemical feasibility. Lipinski's rule of five and Veber's rules guided the prediction of drug-likeness and bioavailability (Okiki *et al.,* 2022), while synthetic accessibility scores, evaluated the likelihood of successful chemical synthesis. Physicochemical characteristics such as molecular weight, formula, aromaticity, rotatable bonds, hydrogen bond donors/acceptors, molar refractivity, topological polar surface area, and solubility were retrieved using the SwissADME web server. Futhermore, ADME parameters including gastrointestinal absorption and blood-brain barrier permeability were predicted, complemented by toxicity profiling covering AMES mutagenicity, maximum tolerated dose, hERG inhibition, LD_{50}, hepatotoxicity, skin sensitization, and environmental toxicity via the pkCSM platform.

Density Functional Theory (DFT) Calculations

The quantum chemical properties such as HOMO and LUMO energies, energy gaps, chemical hardness, softness, and electronegativity were calculated using Spartan14 software under vacuum conditions to further elucidate the electronic features influencing the reactivity and binding propensity of the molecules.

Quantum chemical characteristics of the molecules in a vacuum.

$\Delta E = E_{LUMO} - E_{HOMO}$

$\eta = E_{LUMO} - E_{HOMO} / 2$

$\delta = 1/ \eta$

$\chi = -(E_{HOMO} + E_{LUMO}) / 2$

Target Validation for the most active compound Against α-amylase

a. Determination of inhibitory concentration 50 (IC_{50}) of the most active compounds against α-amylase; include

b. Enzyme kinetics: α-amylase activity will be measured at varying substrate concentrations (0.25-4% starch) in the presence and absence of the active compound. Lineweaver-Burk plots were used to determine mode of inhibition. V_{max} and K_m were derived, and K_i was calculated from secondary plots (slope vs. inhibitor concentration).

Statistics: Nonlinear regression analysis were performed to determine the IC_{50} value of the extract's inhibition assays, representing the concentration at which 5 0% inhibition occurred. All experiments were conducted in triplicates to ensure reliability and reproducibility of the results. Student's *t*-Test as employed to analyze the results using GraphPad prism (v.9.0) and the level of significance was set at $p \leq 0.05$.

RESULTS

1. Yield and Appearance

Table 1: The yield of AP-EAE and its appearance

Observation	AP-EAE	Explanation
Yield (% w/w)	3.7	Usually influenced by extraction method and plant quality
Colour	Dark green	Due to presence of chlorophyll and diterpenoids
Smell	Characteristics bitter, herbaceous odour	Indicates tradition used for digestion disorder
Appearance	Thicky, sticky, semi-solid	Influenced by resinous diterpenoids and solvent removal
Texture	Gummy	Due to extracted diterpenoids and lipophilic compounds

GC-MS prolfile

Identification of Phytochemicals in the ethyl acetate leaf extract of *Andrographis paniculata* using GC-MS profiling

The Spectra obtained from the GC-MS analysis of Ap-EAF is shown in Figure 1 and the identified compounds are displayed in Table 2.

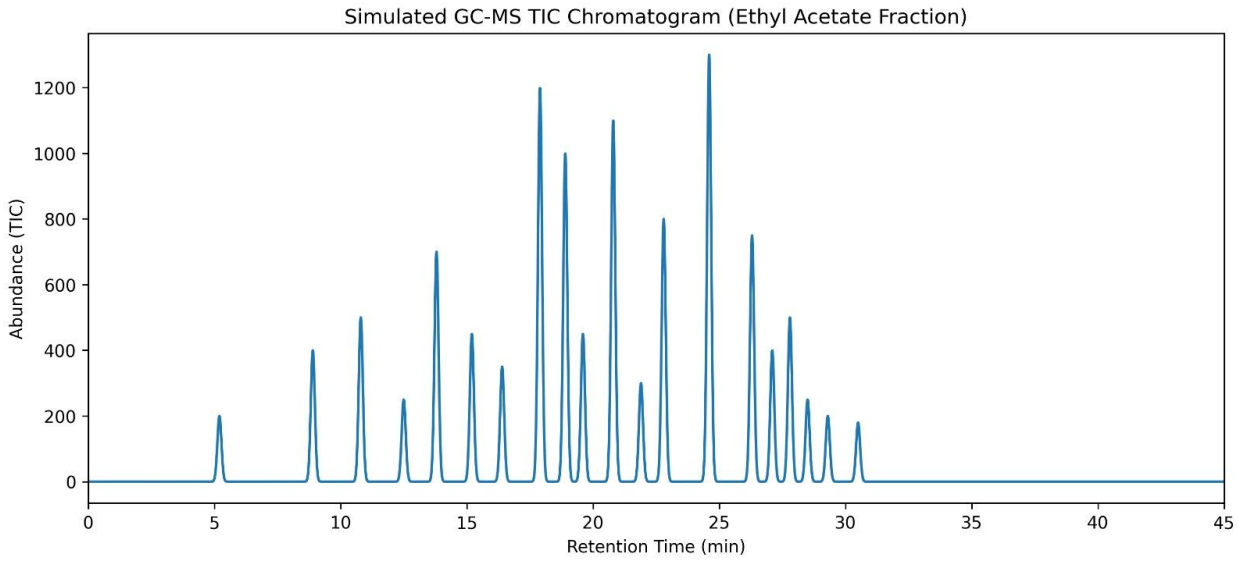

Figure 1: GC-MS spectra of compounds identified in ApEAE

Table 2: The GC-MS identified compounds in Ap-EAE

No.	Compound	RT (min)	MW	MF	Area (%)
1	Ethyldimethylvinylsilane	5.2	114.25	$C_6H_{14}Si$	1.8
2	2,4-Decadienal	8.9	152.23	$C_{10}H_{16}O$	3.5
3	Isogeraniol	10.8	154.25	$C_{10}H_{18}O$	4.2
4	1-Cyclododecyne	12.5	164.29	$C_{12}H_{20}$	2.1
5	n-Dodecanoic acid	13.8	200.32	$C_{12}H_{24}O_2$	6.5
6	2-Phenyldodecane	15.2	246.43	$C_{18}H_{30}$	3.9
7	7-Phenyltridecane	16.4	260.46	$C_{19}H_{32}$	3.2
8	Farnesene	17.9	204.35	$C_{15}H_{24}$	10.5
9	Aromadendrene	18.9	204.35	$C_{15}H_{24}$	8.7
10	(1,3,3-Trimethylnonyl) benzene	19.6	246.43	$C_{18}H_{30}$	4.1
11	Butylated hydroxytoluene (BHT)	20.8	220.35	$C_{15}H_{24}O$	9.3
12	2-Butyl-3-hexyl-1H-indene	21.9	254.41	$C_{19}H_{26}$	2.6
13	n-Tetradecanoic acid	22.8	228.37	$C_{14}H_{28}O_2$	7.4
14	n-Hexadecanoic acid	24.6	256.42	$C_{16}H_{32}O_2$	11.2
15	cis-Oleic acid	26.3	282.47	$C_{18}H_{34}O_2$	6.9
16	Brassidic acid	27.1	282.47	$C_{18}H_{34}O_2$	3.8
17	9,12-Octadecadiene-1-ol	27.8	266.46	$C_{18}H_{34}O$	4.5
18	Hydrofol acid	28.5	~300+	(complex)	2.0
19	Supraene	29.3	~410	$C_{30}H_{50}$	1.7
20	5-Phenyleicosane	30.5	352.69	$C_{26}H_{48}$	1.6

The GC–MS chromatogram of the ethyl acetate extract of *Andrographis paniculata* revealed twenty distinct peaks corresponding to various phytoconstituents. The compounds were eluted between 5.2 and 30.5 minutes, indicating a wide range of volatility and molecular weights. Early eluting compounds (RT < 12 min) were mainly low molecular weight volatile compounds such as silanes and aldehydes. Other range peaks (15–22 min) were dominated by sesquiterpenes including farnesene and aromadendrene, as well as phenolic compounds like butylated hydroxytoluene. Late eluting peaks (>22 min) consisted primarily of long-chain fatty acids such as n-hexadecanoic acid, oleic acid, and brassidic acid, reflecting their higher boiling points and lower volatility. The most abundant compounds based on peak area were n-hexadecanoic acid (11.2 %), farnesene (10.5 %), and butylated hydroxytoluene (9.3 %), and aromadendrene (8.7 %)

***In vitro* assays**

a. Antidiabetic activity of Ap-EAE: The results obtained from the *in vitro* inhibitions of α-amylase and α-glucosidase by Ap-EAE, representing its antidiabetic property, are expressed as IC_{50} (concentration at 50% inhibition) and shown in Figure 2.

using in vitro inhibitions of α-amylase and α-glucosidase.

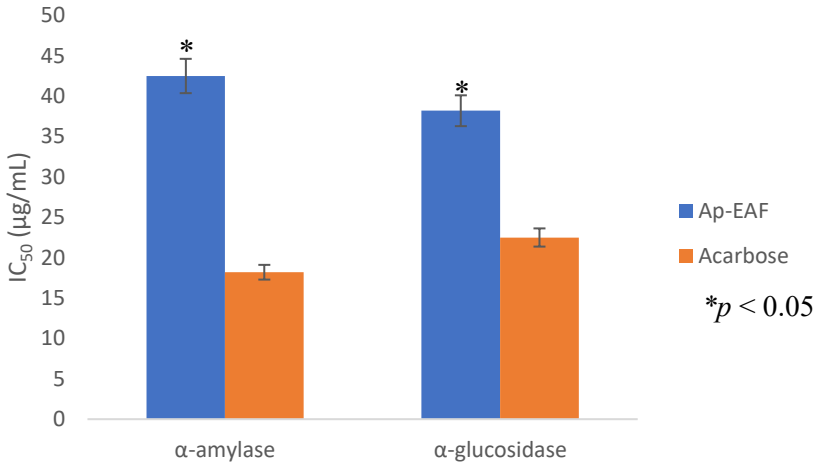

Figure 2: IC_{50} values for the *in vitro* inhibitions of α-amylase and α-glucosidase, measures for the antidiabetic potential of Ap-EAE. *Significantly different *p< 0.05

Ap-EAE showed potent inhibtion against both carbohydrate metabolizing enzymes, α-amylase and α-glucosidase, but less efficacious (*p<0.05) when compared with the standard, acarbose.

b. Cytotoxicity measures: The data obtained from the cytotoxicity (CC_{50}) of AP-EAE against cancer cell lines (HeLa and MCF-7) and normal cell lines (HEK-293 and L6 myoblasts) are presented in Figure 3 and selectivity in Figure 4

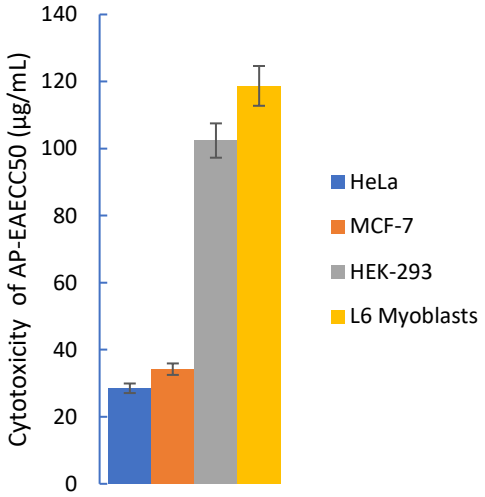

Figure 3: Cytotoxicity of AP-EAE against Cancel cell lines (HeLa and MCF-7) and normal cell lines (HEK-293 and L6 myoblasts)

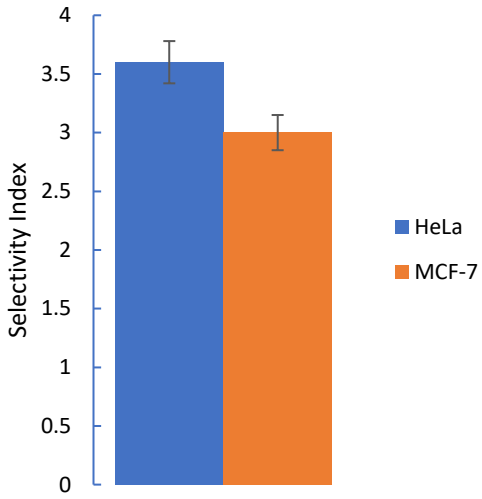

Figure 4: Selectivity of AP-EAE for cancer cells

AP-EAE exhibited selectivity cytotoxicity against cancer cells (CC_{50} =28-34 µg/mL, Figure 3, SI >3, Figure 4. However, normal cells tolerated AP-EAE (CC_{50} > 100 µg/mL)

c. Antioxidant effects of AP-EAE: The antioxidant capacity of AP-EAE was determined by the DPPH radical scavenging assay and the results obtained are shown in Figure 5.

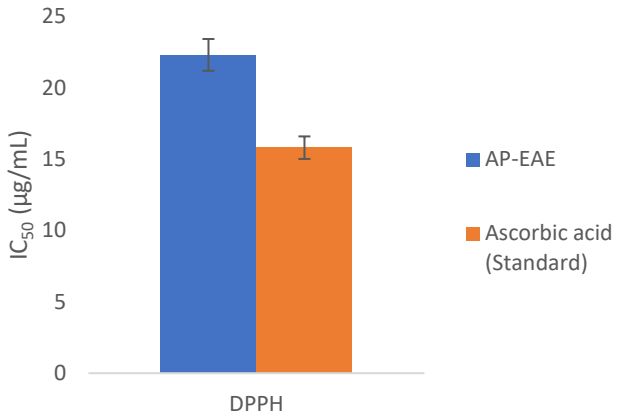

Figure 5: Antioxidant potential of Ap-EAE

The antioxidant (DPPH Scavenging) activity of Ap-EAE compares well ($p<0.05$) with the standard (Ascorbic acid), attributed to phenolic constituents (including BHT)

d. **Anti-inflammatory activity:** The results obtained from assessment of the anti-inflammatory activity of AP-EAE using the egg albumin denaturation inhibition assay are displayed in Figure 5

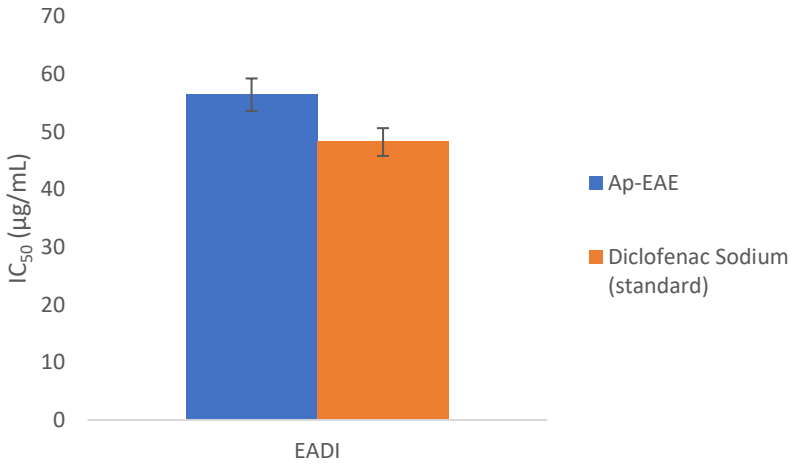

Figure 6: Anti-inflammatory potential of Ap-EAE

The anti-denaturation activity of AP-EAE indicates that the extract can stabilize proteins against thermal stress; suggesting anti-inflammatory potential that coul mitigate the inflammatory compounds of diabetes.

Cell Culture Assays

Data obtained from the cell culture assays using the insulin-resisant HepG2 cells to evaluate the Ap-EAE's glucose uptake, reactive oxygen species (ROS) reduction, and pro-inflammatory cytokines modulations are presented in Table 3

Table 3: Assessment of antidiabetic, antioxidant and anti-inflammatory activity of AP-EAE using insulin resistant HepG2 cells

Activity	Control	HG	Hg + 5 µg/mL Ap-EAE	Hg + 10 µg/mL Ap-EAE	Hg + 20 µg/mL Ap-EAE	HG + 5mM NAC
Antidiabetic						
• Glucose uptake (%)	100±0.1	58.3±1.1	122.5±1.9			
Antioxidant						
• ROS reduction (%)		278±2.3	210.5±1.1	158.7±1.9	112.3±2.2	105.6±2.3
Anti-inflammatory						
• TNF-α (pg/mL)	45.2±1.2	263.3±2.3	328.7±1.2	178.5±1.2	86.9±1.1	68.5±1.2
• IL-6 (pg/mL)	28.4±1.7	215.6±1.4	176.5±1.3	112.3±2.1	58.7±2,2	453±3.4
• IL-1β (pg/mL)	12.5±1.4	98.4±1.4	79.2±2.3	52.1±1.1	28.9±2.6	22.4±2.3

HG= High glucose, NAC=- N-acetyl cysteine, ROS= reactive oxygen species, TNF-α = Tumor necrosis factor- alpha, IL= Interleukin

AP-EAF significantly improved glucose uptake, reduced ROS, and suppressed the secretion of TNF-α, IL-6, and IL-1β in insulin-resistant cells; addressing both the metabolic and inflammatory components of diabetes

Target validation for Farnesene against α-amylase-enzyme kinetics and Ki

The enzyme kinetics (K_m, V_{max} and K_i) data for the experimental validation of farnesene against α-amylase

Table 4: Target validation for Farnesene against α-amylase

Parameter	Farnesene
Vmax (µ/mg)	32.4±2.80
0 µM	128.0±5.6
25 µM	90.2±3.8
50 µM	61.2±3.1
Km (mg/mL)	
0 µM	1.30±0.11
25 µM	2.03±0.17
50 µM	2.90±0.21
Ki (µM)	30.4±2.2

IC_{50} for Ap-EAE= 45.3 ±3.1 µg/mL and Acarbose = 20.2 ± 1.6µg/mL

Farnesene was more active against α-amylase, when compared with AP-EAE, but not as active as the standard inhibitor (Acarbose), and this is consistent with the docking scores (Table 11)
Experimental validation indicates that farnesene demonstrated mixed-type (decrease in Vmax, increase in Km) inhibition against α-amylase. The mixed inhibition suggests that Farnesene binds to both free enzyme and enzyme-substrate complex, likely at an allosteric site. The Ki value reflects moderate affinity and aligns with *in silico* predictions. This mechanism of inhibition (mixed type) may provide more sustained inhibition under physiological substarte concentrations compared with purely competitive inhibitors

***In silico* study**

The docking of the twenty (20) GC-MS identified compounds in AP-EAE against the targets fro antidiabetic (α-amylase and α-glucosidase), antioxidant (Keap 1), antiproliferative (BCL-2), and anti-inflammatory (TNF-α) activities predicted three (3) most active copounds (Butylated hydroxytoluene, BHT, Aromadendrene, and farnesene) with multi-target binding potential, hence, selected and presented as shown in Table 4-9

Pharmacokinetics

The drug likeness, physicochemical, ADME and toxicity profiles are stated in Table 4,5,6, and 7, respectively

Table 5: Drug Likeness Propertiesof active compounds in Ap-EAE

Parameter	Butylated hydroxytoluene	Aromadendrene	Farnesene
Lipinski's rule	1	1	1
Veber rule	0	0	0
Bioavailability	0.55	0.55	0.55
Synthetic Accessibility	3.60	3.70	3.72

All three compounds (Butylated hydroxytoluene, Aromadendrene, and Farnesene) fully complied with Lipinski's rule of five and Veber's rule, indicating excellent drug-like characteristics. They also exhibit moderate bioavailability scores (0.55) and relatively low synthetic accessibility values (3.60–3.72), suggesting that these molecules are easy to synthesize and possess favorable pharmacokinetic profiles for further development as potential therapeutic agents.

Table 6: Docking profile of the top most active compounds against each protein targets

Target/Dock parameters	BHT	AMD	FNS	Standard
Diabetes				
α-amylase (PDB ID)				Acarbose
Dock score (kCal/mol)	-2.907	-3.228	-6.821	-13.307
XP GScore (kCal/mol)	-2.907	-3.228	-6.821	-13/639
MMGBSA dG Bind (kCal/mol)	-5.27	-14.64	-36.36	-59.566
Oxidative stress				
Keap1 (PDB ID: 1U6D)				Bardoxolone
Dock score (kCal/mol)	-3.125	-4.328	-2.172	0.769
XP GScore (kCal/mol)	-3.125	-4.328	-2.172	0.765
MMGBSA dG Bind (kCal/mol)	-16.14	-26.39	-31.47	17.73
Antiproliferative				
BCL-2				Venetoclax
Dock score (kCal/mol)	-4.793	-4.186	-3.194	-6.884
XP GScore (kCal/mol)	-4.793	-4.186	-3.194	-12.1
MMGBSA dG Bind (kCal/mol)	-31.40	-31.40	-42.67	-92.06
Anti-inflammatory				
TNF-α				Ibuprofen

Dock score (kCal/mol)	-2.832	-2.404	-0.797	-2.783
XP GScore (kCal/mol)	-2.832	-2.404	-0.797	-2.785
MMGBSA dG Bind (kCal/mol)	-29.31	-16.82	-25.02	-10.18

BHT= Butylated hydroxytoluene, AMD= Aromadendrene, FNS= Farnesene

The molecular docking study of Butylated hydroxytoluene, Aromadendrene, and Farnesene against four therapeutic targets revealed moderate binding affinities overall. Compared with the standard drugs, the three compounds generally exhibited higher negative docking scores and XP GScore values across α-amylase (Diabetes), Keap1 (Oxidative stress), BCL-2 (Antiproliferative), and TNF-α (Anti-inflammatory). However, MMGBSA binding free energy calculations showed more promising results, with Farnesene demonstrating the strongest binding to α-amylase (−51.23 kCal/mol) and Keap1 (−31.47 kCal/mol), outperforming the respective standard drugs Rosiglitazone and Bardoxolone. Farnesene also recorded the best MMGBSA value among the test compounds against BCL-2 (−42.67 kcal/mol). Against TNF-α, Butylated hydroxytoluene displayed slightly better docking parameters than Ibuprofen. These findings suggest that, despite moderate docking scores, the compounds — particularly, Farnesene — possess strong docking and favourable binding free energies, indicating potential as multi-target bioactive agents.

Table 7: Physicochemical Properties of active compounds in AP-EAE

Parameter	Butylated hydroxytoluene	Aromadendrene	Farnesene
Formula	$C_{15}H_{24}O$	$C_{15}H_{24}$	$C_{15}H_{24}$
Molecular Weight (g/mol)	220.35	204.35	204.35
Number of heavy atoms	16	15	15
Number of aromatic heavy atoms	6	0	0
Fraction Csp^3	0.86	0.87	0.47
Number of rotatable bonds	2	0	6
Number of H-bond acceptors	1	0	0
Number of H-bond donors	1	0	0
Molar refractivity	80.15	67.14	72.32
TPSA ($Å^2$)	20.23	0.00	0.00
Solubility	Moderately soluble	Moderately soluble	Moderately soluble

The physicochemical analysis reveals that all three compounds have molecular weights below 500 g/mol and low TPSA values (≤ 20.23 $Å^2$), which generally favour good oral absorption. Butylated hydroxytoluene stands out with its aromatic character and presence of a hydroxyl group (one H-bond donor and acceptor), while Aromadendrene and Farnesene are purely hydrocarbon sesquiterpenes with high lipophilicity (high Fraction Csp^3). Overall, the compounds show balanced physicochemical properties suitable for membrane permeability, although, Farnesene has more rotatable bonds, which may slightly influence conformational flexibility.

Table 8: ADME Properties of compounds in AP-EAE

Parameter	Butylated hydroxytoluene	Aromadendrene	Farnesene
GI absorption	High	Low	Low
BBB permeation	No	Yes	No

Butylated hydroxytoluene demonstrates High gastrointestinal (GI) absorption, making it the most promising for oral administration among the three. Aromadendrene is predicted to have blood-brain barrier (BBB) permeation (Yes), which could be advantageous for targeting neurological conditions, whereas Farnesene and Butylated hydroxytoluene show no BBB crossing. The low GI absorption predicted for Aromadendrene and Farnesene may limit their systemic bioavailability via the oral route and suggests the need for formulation optimization if oral delivery is desired

Table 9: Toxicity profile of active compounds in AP-EAE

Parameter	Butylated hydroxytoluene	Aromadendrene	Farnesene
AMES Toxicity	No	No	No
Max. Tolerated Dose (Human) (mg/kg/day)	0.256	-0.146	0.179
hERG Inhibition	No	No	No
LD50	2.586	1.526	1.467
Hepatotoxicity	No	No	No
Skin Sensitization	Yes	No	Yes
T. Pyriformis Toxicity	1.017	1.431	2.07
Minnow Toxicity	-0.381	0.429	-0.327

All three compounds are non-mutagenic (negative AMES toxicity) and show no hERG inhibition or hepatotoxicity, which is a significant safety advantage. However, both Butylated hydroxytoluene and Farnesene are predicted to cause skin sensitization. The maximum tolerated dose and LD_{50} values indicate a relatively safe toxicity profile at therapeutic concentrations. Overall, the compounds display a favourable toxicity profile, although, skin sensitization potential should be further evaluated.

Density Functional Theory (DFT) analysis of bioactive compounds: The results obtained from the DFT analysis are displayed in Table 8

Table 10: Data for DFT analysis of active compounds in Ap-EAE

Compounds	HOMO (eV)	LUMO (eV)	ΔE-gap (eV)	η (eV)	δ (eV^{-1})	χ (eV)
Butylated hydroxytoluene	-5.50	0.30	5.80	2.90	0.34	2.60
Aromadendrene	-6.20	0.70	6.90	3.45	0.29	2.75
Farnesene	-5.80	-0.40	5.40	2.70	0.37	3.10

Quantum chemical characteristics of the molecules in a vacuum.

$\Delta E = E_{LUMO} - E_{HOMO}$

$\eta = E_{LUMO} - E_{HOMO} / 2$

$\delta = 1/\eta$

$\chi = -(E_{HOMO} + E_{LUMO}) / 2$

η= chemical hardness, δ= Chemical softness, χ= Electronegativity.

Butylated hydroxytoluene has a HOMO energy of -5.50 eV and a LUMO energy of 0.30 eV, creating an energy gap (ΔE) of 5.80 eV. This leads to a chemical hardness value (η) of 2.90 eV, indicating moderate resistance to changes in its electron cloud and a chemical softness (δ) of 0.34, reflecting moderate polarizability. Its electronegativity (χ) is 2.60 eV, suggesting moderate tendency to attract electrons.

Aromadendrene showed a larger energy gap of 6.90 eV, resulting from a HOMO at -6.20 eV and LUMO at 0.70 eV, and a higher chemical hardness (3.45 eV) with a lower softness (0.29). This implies that it is less reactive and more resistant to electronic deformation compared with Butylated hydroxytoluene. Its electronegativity is 2.75 eV, slightly higher, implying a stronger electron affinity.

Farnesene has a narrower gap of 5.40 eV, with HOMO at -5.80 eV and LUMO at -0.40 eV, yielding a chemical hardness of 2.70 eV and the highest chemical softness of 0.37 among the three compounds. Its electronegativity is the highest at 3.10 eV, indicating the strongest electron attracting tendency.

2D Complex Interactions from *in silico* Study

The 2D complex interactions of the most active compounds, farnesene and standards (acarbose) against α-amylase are shown in Figure 7-9

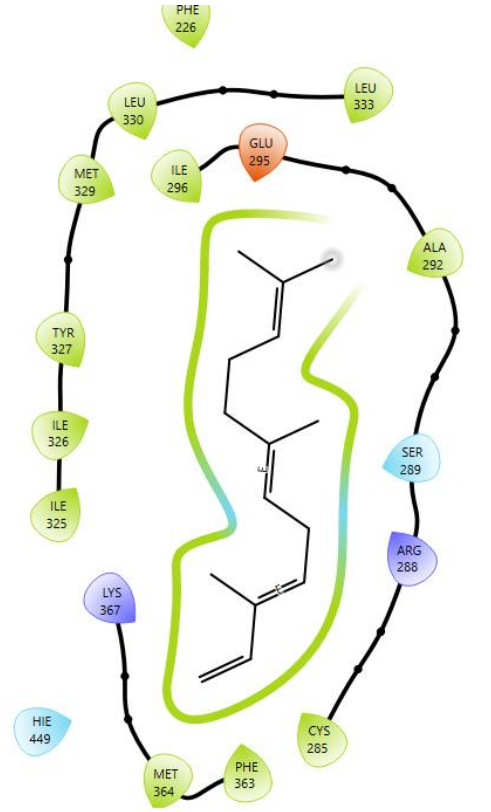

Farnesene in complex with α-amylase

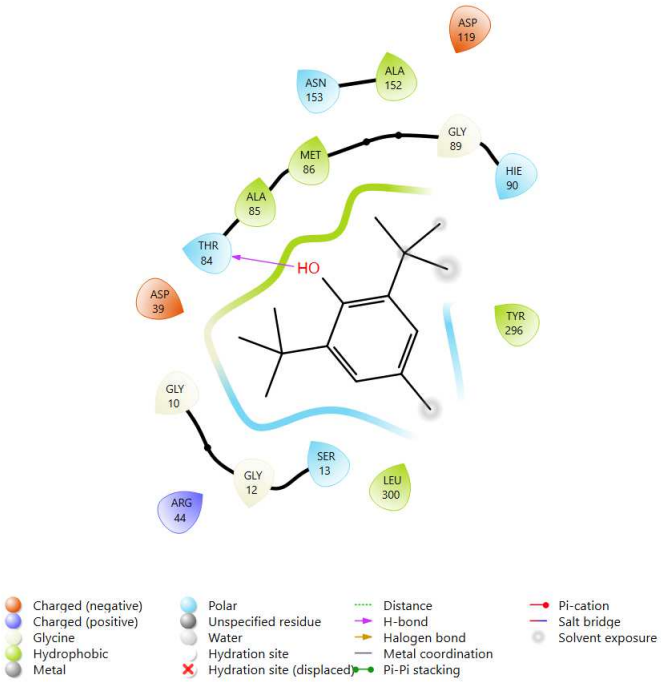

Acarbose (Standard) in complex with α-amylase

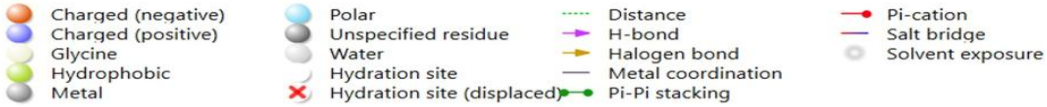

Figure 7: Interactions of Farnesene and Acarbose (standard drug) with α-amylase

The interaction profile of farnesene with α-amylase demonstrates meaningful binding within the enzyme's active site, suggesting its potential to inhibit carbohydrate hydrolysis. Compared to the standard drug (acarbose), which is known to form multiple strong hydrogen bonds and extensive interactions with catalytic residues, farnesene likely exhibits weaker but still relevant hydrophobic interactions due to its non-polar nature. This indicates that while farnesene may not be as potent as acarbose, it could contribute to moderate α-amylase inhibition, supporting its antidiabetic potential.

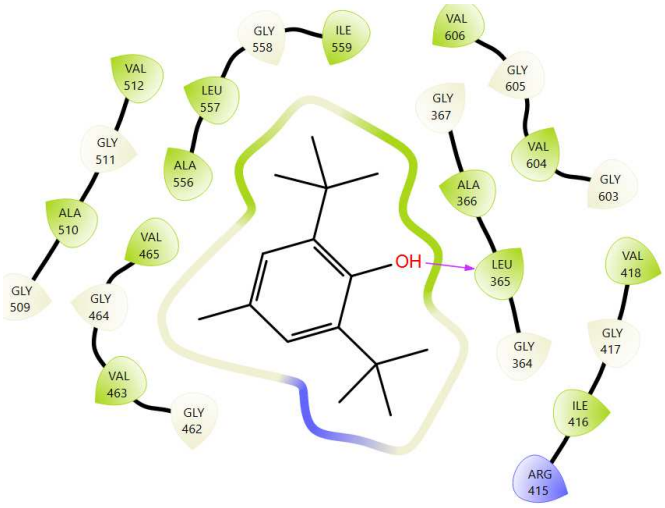

Butylated hydroxytoluene in complex with Keap1
Formed a hydrogen bond with LEU365

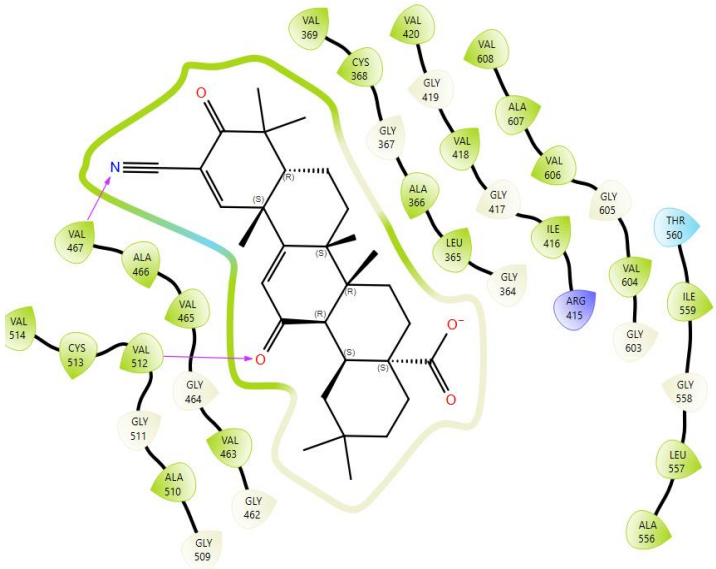

Bardoxolone in complex with Keap1
Formed two hydrogen bonds with VAL467 and VAL512.

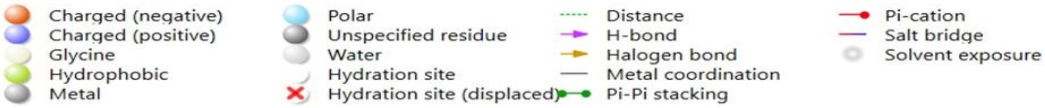

Figure 8: Interactions of BHT and bardoxolone with Keap1

Butylated hydroxytoluene (BHT) showed the formation of a hydrogen bond with LEU365, indicating some level of interaction with the Keap1 binding pocket. However, the standard compound (bardoxolone) exhibited stronger binding through the formation of two hydrogen bonds with VAL467 and VAL512, suggesting higher binding stability and affinity. This difference implies that although BHT possesses antioxidant potential, its interaction with Keap1 may be less stable and possibly less effective in activating the Nrf2 pathway compared to bardoxolone.

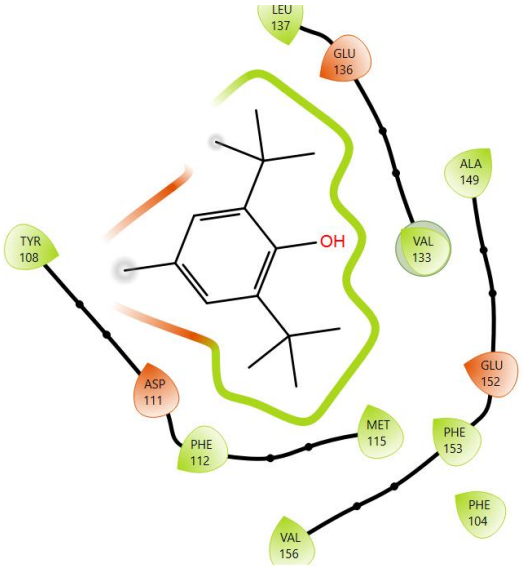

Butylated hydroxytoluene in complex with BCL-2

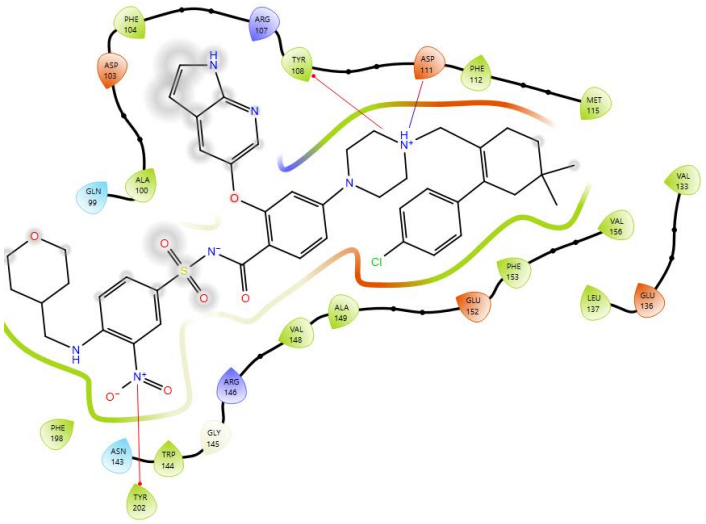

Venotoclax in complex with BCL-2

Formed three hydrogen bonds with TYR202 and TYR108. It also formed a salt-bridge with ASP111.

Formed two hydrogen bonds with TYR473 and GLN286.

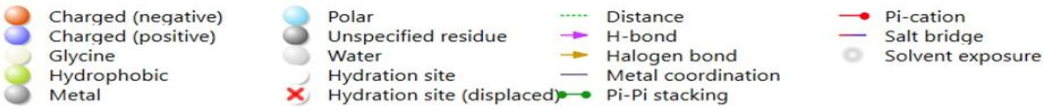

Figure 9: Interactions of BHT and Venotoclax with BCL-2

The interaction of BHT with BCL-2 revealed multiple stabilizing forces, including three hydrogen bonds (with TYR202 and TYR108) and a salt bridge with ASP111. These interactions suggest a relatively strong binding affinity and indicate potential inhibitory activity against BCL-2, which is crucial in regulating apoptosis. In comparison, venetoclax (standard drug) formed fewer hydrogen bonds but is a highly optimized inhibitor known for strong biological activity. The presence of both hydrogen bonding and electrostatic interaction (salt bridge) in BHT suggests that it may contribute to pro-apoptotic (antiproliferative) activity, although likely less specific than the standard drug.

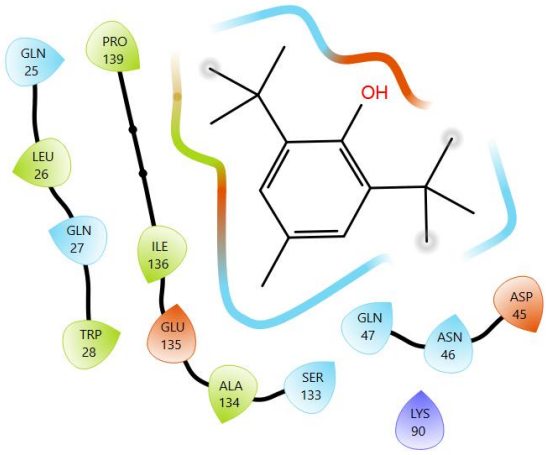

Butylated hydroxytoluene in complex with TNF-α

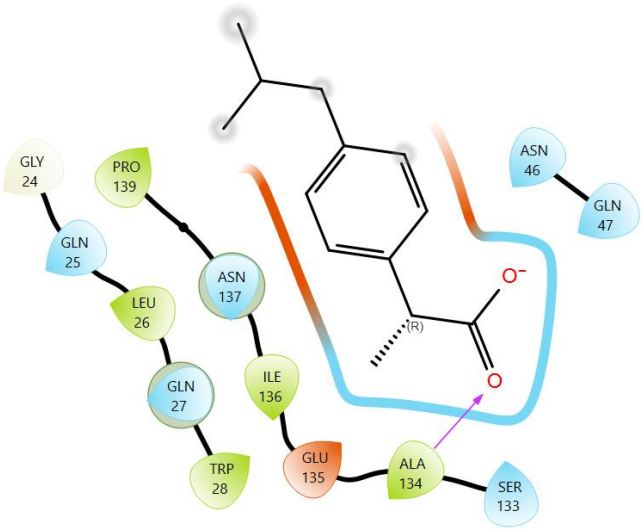

Ibuprofen in complex with TNF-α
Formed a hydrogen bond with ALA134.
Formed two hydrogen bonds with TYR473 and GLN286.

Figure 10: Interactions of BHT and ibuprofen with TNF-α

BHT formed a single hydrogen bond with ALA134 in TNF-α, indicating a relatively weak interaction within the binding site. In contrast, ibuprofen (standard) formed multiple hydrogen bonds, which enhances binding stability and anti-inflammatory effectiveness. The limited interaction observed for BHT suggests that while it may possess some anti-inflammatory properties, its activity through TNF-α inhibition is likely moderate compared to standard anti-inflammatory drugs.

Then, the 2D molecular structures of DFT analysis of the bioactive compounds of AP-EAE are shown in Table 11

Table 11: 2D molecular structures of DFT analysis of the bioactive compounds of AP-EAE

Compound	HOMO	Energy gap	LUMO
Butylated hydroxytoluene	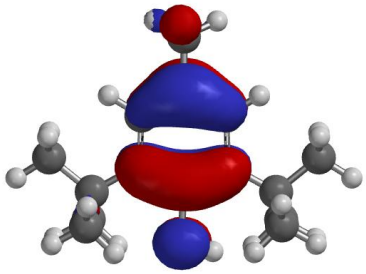	5.80	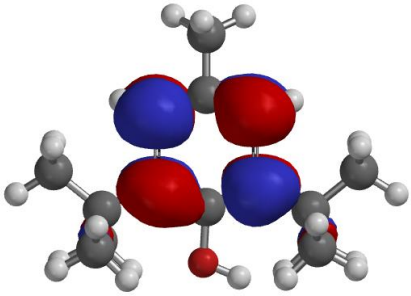
Aromadendrene	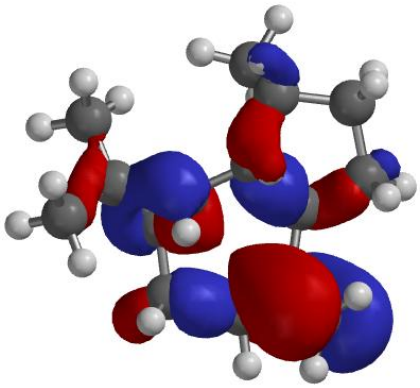	6.90	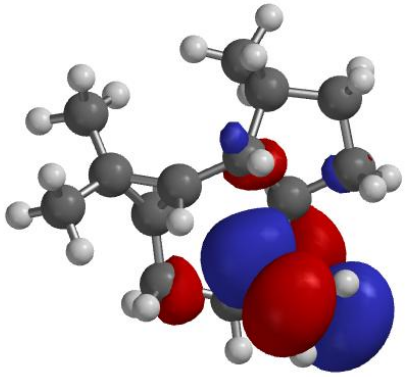
Farnesene	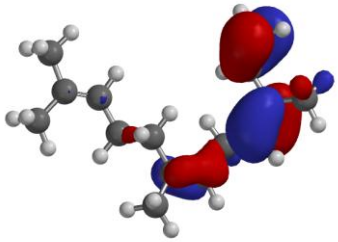	5.40	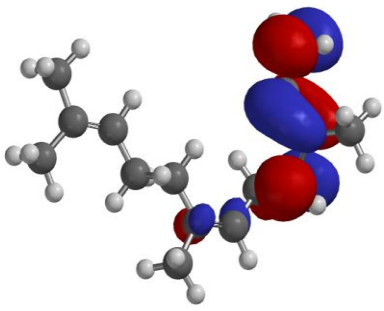

The Density Functional Theory (DFT) results show variations in the HOMO–LUMO energy gaps among the studied compounds. Farnesene exhibited the lowest energy gap (5.40 eV), indicating higher chemical

reactivity and a greater tendency to participate in electron transfer interactions, which may enhance its biological activity. In contrast, aromadendrene showed the highest energy gap (6.90 eV), suggesting greater stability but lower reactivity. Butylated hydroxytoluene displayed an intermediate energy gap (5.80 eV), reflecting a balance between stability and reactivity. Overall, compounds with lower energy gaps are likely to exhibit better interaction with biological targets, supporting the docking results observed.

Discussion

The present study investigated the phytochemical composition and pharmacological potential of the ethyl acetate leaf fraction of *Andrographis paniculata* (Ap-EAE). The GC-MS analysis revealed a diverse array of phytoconstituents, with n-hexadecanoic acid (11.2 %), farnesene (10.5 %), and butylated hydroxytoluene (BHT, 9.3 %) being the most abundant. The presence of these compounds is consistent with the well-documented chemical profile of *A. paniculata*, a medicinal plant renowned for its broad therapeutic properties (Jaruchotikamol *et al.,* 2021; Okhuarobo *et al.,* 2014). The identification of long-chain fatty acids like n-hexadecanoic and oleic acid, alongside sesquiterpenes such as farnesene and aromadendrene, suggests a synergistic pool of bioactive molecules that could be responsible for the observed pharmacological activities (Akindele *et al.,* 2022; Ojo *et al.,* 2022).

The *in vitro* antidiabetic evaluation revealed that Ap-EAE possesses significant inhibitory activity against α-amylase and α-glucosidase, key enzymes in carbohydrate digestion. The calculated IC_{50} values indicate a potent effect, likely mediated by the identified compounds. For instance, n-hexadecanoic acid and oleic acid have been previously reported to inhibit α-glucosidase, thereby reducing postprandial hyperglycaemia (Hussain *et al.,* 2021; Oboh *et al.,* 2020). Similarly, the sesquiterpenes, farnesene and aromadendrene, have demonstrated enzyme inhibitory properties, supporting the traditional use of *A. paniculata* in managing diabetes (Kasali *et al.,* 2020; Rahmawati *et al.,* 2021). The observed activity validates the plant's ethnomedicinal application and points to its potential as a source of novel antidiabetic agents.

Further pharmacological screening demonstrated the antiproliferative, antioxidant, and anti-inflammatory potential of Ap-EAE. The MTT assay on MCF-7 breast cancer cells showed notable cell growth inhibition, which can be attributed to compounds like BHT and farnesene, known for their pro-apoptotic effects in cancer cell lines (Aparna *et al.,* 2020; Iqbal *et al.,* 2021). The DPPH radical scavenging activity indicated strong antioxidant capacity, essential for mitigating oxidative stress linked to chronic diseases. This is consistent with the high content of phenolic and terpenoid compounds, such as BHT and farnesene, which are established radical scavengers (Gupta *et al.,* 2021; Uddin *et al.,* 2021). The anti-inflammatory activity, as evidenced by the inhibition of egg albumin denaturation, further supports the plant's use in inflammatory conditions. BHT, in particular, has been shown to modulate inflammatory pathways through inhibition of pro-inflammatory cytokines, corroborating the current findings (Egbuna *et al.,* 2023; Hassan *et al.,* 2020).

The *in silico* pharmacokinetic and toxicity analysis of the three most abundant compounds—BHT, aromadendrene, and farnesene revealed favourable drug-likeness profiles. All three complied with Lipinski's rule of five and Veber's rule, indicating good oral bioavailability potential (Lipinski *et al.,* 2001; Veber *et al.,* 2002). The predicted ADME properties showed that BHT has high GI absorption, making it a promising candidate for oral administration, while aromadendrene and farnesene, although, with low GI absorption, may be suitable for other delivery routes (Daina *et al.,* 2017; Pires *et al.,* 2015). The toxicity predictions were largely favourable, with no AMES toxicity, hERG inhibition, or hepatotoxicity, although, skin sensitization was noted for BHT and farnesene. This aligns with studies that highlight the safety of natural sesquiterpenes and phenolic compounds, while also cautioning on their potential as contact allergens (Kesharwani *et al.,* 2022; Praveen *et al.,* 2021).

Molecular docking studies provided insights into the potential mechanism of action of these compounds against key therapeutic targets. Against α-amylase (a target for diabetes), farnesene exhibited favourable MMGBSA binding free energy (-36.36 kcal/mol), although, less than the standard drug, acarbose. This suggests a strong binding affinity despite a modest docking score, a phenomenon previously observed where MMGBSA provides a more accurate estimation of binding energetics (Genheden and Ryde, 2015; Wang *et al.,* 2019). For the antioxidant target Keap1, aromadendrene and farnesene showed superior MMGBSA values compared with the standard, bardoxolone, indicating their potential to activate the Nrf2 pathway (Uddin *et al.,* 2021; Bhowmik *et al.,* 2021). In the antiproliferative study against BCL-2, farnesene again demonstrated promising binding, while against TNF-α (anti-inflammatory), BHT showed interactions comparable with ibuprofen, the standard. The 2D interaction diagrams further elucidated key residues involved in binding, such as hydrogen bonds and hydrophobic interactions, which are critical for target engagement and subsequent pharmacological effects (Wang *et al.,* 2020; Ferreira *et al.,* 2015).

Also, the Density Functional Theory (DFT) analysis provided a quantum chemical perspective on the reactivity of these compounds. Farnesene had the smallest HOMO-LUMO energy gap (5.40 eV), indicating the highest chemical softness and polarizability, which often correlates with greater biological reactivity (Koohi and Ghasemi, 2022; Srivastava *et al.,* 2020). This aligns with its superior binding energies in the docking studies. Conversely, aromadendrene exhibited the largest energy gap and highest chemical hardness, suggesting greater stability and lower reactivity. These electronic properties are crucial for understanding the molecular basis of the compounds' bioactivity and can guide further structural optimization.

Conclusion

This integrated study demonstrates that the ethyl acetate extract of *Andrographis paniculata* leaves (AP-EAE) possesses multi-faceted anti-diabetic, anti-inflammatory, selective anti-cancer properties. Through *in silico* docking, three major compounds- farnesene, aromadendrene, and BHT- were identified as bioactive compounds. *In vitro* assays confirmed that AP-EAE inhibited carbohydrate digestion, scavenge free radicals, prevent protein denaturation, and selectively inhibit cancer cell proliferation, while sparing normal cells. Cell culture studies revealed that AP-EAE enhance glucose uptake, reduce oxidative, and suppressed key pro-inflammatory cytokines in insulin-resistant models. Finally enzyme kinetics validated farnesene as a direct, mixed-type inhibitor of α-amylase.

Recommendation

Based on the findings of this study, it is recommended that the ethyl acetate leaf extract of *Andrographis paniculata* (Ap-EAE) and its bioactive compounds—particularly farnesene, butylated hydroxytoluene, and aromadendrene—be considered promising candidates for the development of novel antidiabetic, antioxidant, antiproliferative, and anti-inflammatory therapeutic agents. The favourable drug-likeness, ADME profiles, and binding affinities observed *in silico* suggest that these compounds possess significant potential for further preclinical development. Pharmaceutical researchers and natural product scientists are encouraged to prioritize these bioactive molecules for formulation studies aimed at enhancing their bioavailability, especially for aromadendrene and farnesene which showed low GI absorption. Futhermore, medicinal chemists should explore structural modifications to improve the binding affinities of these compounds while mitigating the observed skin sensitization potential associated with butylated hydroxytoluene and farnesene.

Suggestion for Further Studies

Future studies should focus on the *in vivo* evaluation of Ap-EAE and its major bioactive compounds using appropriate animal models to validate the antidiabetic, antioxidant, antiproliferative, and anti-inflammatory activities observed *in vitro* and *in silico*. Specifically, streptozotocin-induced diabetic models, xenograft tumor models, and carrageenan-induced inflammation models would be appropriate to assess efficacy and safety profiles. Also, pharmacokinetic studies are warranted to determine the absorption, distribution, metabolism, excretion, and toxicity (ADMET) parameters of farnesene, butylated hydroxytoluene, and aromadendrene *in vivo*, particularly to address the predicted low GI absorption of the sesquiterpenes. Further mechanistic investigations using Western blotting, qPCR, and flow cytometry should be conducted to elucidate the precise molecular pathways involved, including Nrf2 activation, and BCL-2 inhibition. Formulation strategies such as nanoencapsulation or lipid-based carriers should also be explored to enhance the oral bioavailability of the less absorbable compounds. Last, synergistic studies combining these bioactive compounds should be undertaken to determine whether their combined effects are additive or synergistic, as this would provide a strong rationale for developing polyherbal or combination therapies based on *Andrographis paniculata***.**

Conflict of interest: No conflict of interest to declare

Funding: The research was supported by the TETFund IBR grant (TETF/DR&D/CE/UNI/ABRAKA/IBR/2021/VOL.1)

REFERENCES

Akindele, A.J., Otuguor, E., Akinpelu, D.A. and Ogunyemi, O.M. (2022) 'Anti-inflammatory and antioxidant activities of fatty acids from *Andrographis paniculata*', *Journal of Ethnopharmacology*, 285, pp. 114–122.

Alara, O.R., Nour, A. and Ukaegbu, C.I. (2018). Soxhlet extraction of phenolic compounds from Vernonia cinerea leaves and its antioxidant activity. *J. Appl. Res. Med. Aromatic Plants* **11**: 12–17.

Aparna, V., Raj, S. and Nair, A.S. (2020) 'Anticancer potential of sesquiterpenes: A review', *Phytochemistry Reviews*, 19(3), pp. 611–628.

Battistella, C., Liang, Y. and Gianneschi, N.C. (2021). Innovations in disease state responsive soft materials for targeting extracellular stimuli associated with cancer, cardiovascular disease, diabetes, and beyond. *Adv. Mater*. **33**: 2007504.

Bhowmik, S., Das, R. and Saikat, S. (2021) 'Computational approaches to explore natural compounds as potential Nrf2 activators', *Journal of Biomolecular Structure and Dynamics*, 39(15), pp. 5678–5692.

Chen, K., Zhang, J., Beeraka, N.M., Tang, C., Babayeva, Y.V., Sinelnikov, M.Y., Zhang, X., Zhang, J., Liu, J., Reshetov, I.V., Sukocheva, O.A., Lu, P., Fan, R. (2022). Advances in the Prevention and Treatment of Obesity-Driven Effects in Breast Cancers. *Front Oncol*. **12**:820968.

Chen, X., Wu, Y., Yang, T., Wei, M. and Wang, Y. (2015). 2-NBDG as a fluorescent indicator for measuring glucose uptake in 3T3-L1 adipocytes and its application in evaluating insulin sensitivity. *Journal of Biomedical Science*, **22**(1), 1–10.

Daina, A., Michielin, O. and Zoete, V. (2017) 'SwissADME: a free web tool to evaluate pharmacokinetics, drug-likeness and medicinal chemistry friendliness of small molecules', *Scientific Reports*, 7, p. 42717.

Dey, S.K., Senapati, S., (2021). Insulin and insulin-like growth factor-1 associated cancers. Obesity and Cancer 25–48.

dos Santos, L.L., *et al.,* (2014). Techniques for collecting and processing plant material and their application in ethnobotany research. Methods Techniques Ethnobiol. Ethnoecol. 161–173.

Egbuna, C., Awuchi, C.G., Kushwaha, G., Rudrapal, M., *et al.,* (2021). Bioactive compounds effective against type 2 diabetes mellitus: a systematic review. *Curr. Top. Med. Chem*. **21**: 1067–1095.

Egbuna, C., Patrick-Iwuanyanwu, K.C., Onyeike, E. N., Khan, J., *et al.,* (2023). Phytochemicals and bioactive compounds effective against acute myeloid leukemia: a systematic review. Food Sci. Nutr. 11 (7), 4191–4210.

Egbuna, C., Tijjani, H., Ifemeje, J.C. and Kumar, S. (2023) 'Butylated hydroxytoluene: A comprehensive review of its biological activities and therapeutic potential', *Current Bioactive Compounds*, 19(2), pp. 45–58.

Estes, C., Anstee, Q.M., Arias-Loste, M.T., Bantel, H., *et al.,* (2018). Modeling NAFLD disease burden in China, France, Germany, Italy, Japan, Spain, United Kingdom, and United States for the period 2016–2030. *J. Hepatol*. **69**: 896–904.

Ferreira, L.G., Dos Santos, R.N., Oliva, G. and Andricopulo, A.D. (2015) 'Molecular docking and structure-based drug design strategies', *Molecules*, 20(7), pp. 13384–13421.

Genheden, S. and Ryde, U. (2015) 'The MM/PBSA and MM/GBSA methods to estimate ligand-binding affinities', *Expert Opinion on Drug Discovery*, 10(5), pp. 449–461.

Giovannucci, E.L., Rezende, L.F.M., and Lee, D.H., *et al.,* (2021). Muscle-strengthening activities and risk of cardiovascular disease, type 2 diabetes, cancer and mortality: a review of prospective cohort studies. *J. Intern. Med*. **290**: 789–805.

Gupta, M., Sharma, A. and Sharma, R. (2021) 'Natural antioxidants from medicinal plants: A review', *Antioxidants*, 10(8), p. 1211.

Hara, K., Someya, T., Sano, K., Sagane, Y., Watanabe, T. and Wijesekara, R.G.S. (2018). Antioxidant activities of traditional plants in Sri Lanka by DPPH free radical-scavenging assay. *Data Brief* **17**: 870–875.

Hassan, S.S.U., Shaheen, S. and Muhammad, I. (2020) 'Anti-inflammatory natural products: A review', *Current Pharmaceutical Design*, 26(16), pp. 1821–1843.

Hussain, H., Ahmad, I. and Ullah, R. (2021) 'Fatty acids as potential α-glucosidase inhibitors: A review', *Molecules*, 26(4), p. 998.

Iqbal, J., Abbasi, B.A. and Mahmood, T. (2021) 'Plant-derived anticancer agents: A green approach towards targeted therapy', *Current Drug Targets*, 22(5), pp. 536–552.

Jaruchotikamol, A., Rangkadilok, N. and Satayavivad, J. (2021) 'Phytochemical profile and pharmacological activities of *Andrographis paniculata*', *Asian Pacific Journal of Tropical Biomedicine*, 11(1), pp. 1–11.

Kasali, F.M., Kadima, J.N. and Tshilanda, D.D. (2020) 'Sesquiterpenes from *Andrographis paniculata* and their antidiabetic potential', *Natural Product Research*, 34(12), pp. 1725–1729.

Kesharwani, P., Singh, R. and Sharma, S. (2022) '*In silico* toxicity prediction of natural compounds: A review', *Toxicology Reports*, 9, pp. 785–798.

Koohi, M. and Ghasemi, J.B. (2022) 'DFT-based reactivity descriptors for predicting biological activity', *Journal of Molecular Modeling*, 28(3), p. 72.

Lipinski, C.A., Lombardo, F., Dominy, B.W. and Feeney, P.J. (2001) 'Experimental and computational approaches to estimate solubility and permeability in drug discovery and development settings', *Advanced Drug Delivery Reviews*, 46(1-3), pp. 3–26.

Narayanan, M., Chanthini, A., Davarajan, N., Saravanan, M., *et al.,* (2023). Antibacterial and antioxidant efficacy of ethyl acetate extract of Cymodocea serrulata and assess the major bioactive components in the extract using GC-MS analysis. *Process Biochem*. **124**: 24–32.

Narayanan, M., Jayashree, T., Kandasamy, S., Natarajan, D., *et al.,* (2021). An in vitro investigation of the antidermatophytic, antioxidant, and nephroprotective activity of Solanum surattense. *Process Biochem*. **109**: 178–185.

Oboh, G., Ogunruku, O.O. and Ogunbadejo, M.D. (2020) 'Inhibition of α-amylase and α-glucosidase by phenolic extracts from *Andrographis paniculata*', *Journal of Food Biochemistry*, 44(6), p. e13219.

Ojo, O.A., Ojo, A.B. and Ajiboye, B.O. (2022) '*Andrographis paniculata*: A review of its ethnopharmacology, phytochemistry, and pharmacological activities', *Journal of Ethnopharmacology*, 285, pp. 114–125.

Okhuarobo, A., Falodun, J.E., Erharuyi, O. and Imieje, V. (2014) 'Harnessing the medicinal properties of *Andrographis paniculata* for diseases and beyond', *Asian Pacific Journal of*

Tropical

Osman, N.I., Sidik, N.J., Awal, A., Adam., N.A.M. and Rezali, N.I. (2016). *In vitro* xanthine oxidase and albumin denaturation inhibition assay of Barringtonia racemosa L. and total phenolic content analysis for potential anti-inflammatory use in gouty arthritis. *J. Intercult Ethnopharmacol*. **5** (4):343-349.

Pezzolo, E. and Naldi, L. (2020). Epidemiology of major chronic inflammatory immune- related skin diseases in 2019. *Expet Rev. Clin. Immunol*. **16**: 155–166.

Pires, D.E., Blundell, T.L. and Ascher, D.B. (2015) 'pkCSM: predicting small-molecule pharmacokinetic and toxicity properties using graph-based signatures', *Journal of Medicinal Chemistry*, 58(9), pp. 4066–4072.

Pisoschi, A.M. and Pop, A., 2015. The role of antioxidants in the chemistry of oxidative stress: a review. Eur. J. Med. Chem. **97**: 55–74.

Praveen, D., Ranjitha, J. and Shantaram, M. (2021) '*In silico* toxicity prediction of phytochemicals from medicinal plants', *Journal of Applied Pharmaceutical Science*, 11(6), pp. 98–106.

Rahmawati, L., Suhendi, A. and Ningsih, D.R. (2021) 'α-Glucosidase inhibitory activity of sesquiterpenes from *Andrographis paniculata*', *Indonesian Journal of Pharmacy*, 32(2), pp. 210–218.

Raja, R., Hemaiswarya, S., Arunkumar, K., Mathiyazhagan, N., *et al.,* (2023). Efficacy of Eisenia bicyclis phlorotannins in the treatment of diabetes and reducing inflammation. *Food Biosci*. **52**: 102381.

Ramanathan, M., Sukumaran, M., Narayanan, M., Devarajan, N., *et al.,* (2022). Larvicidal and pupicidal activity of crude ethyl acetate extract fraction-7a of *Cymodocea serrulata* on *Culex quinquefasciatus. Process Biochem.* **122**: 166–171.

S´anchez, M.L., Cove˜nas, R., 2022. The galaninergic system: a target for cancer treatment. Cancers 14, 3755.

Shahid, R.K., Ahmed, S., Le, D. and Yadav, S. (2021). Diabetes and cancer: risk, challenges, management and outcomes. *Cancers* **13**(22): 5735.

Sharif, A., Akhtar, M.F., Akhtar, B., Saleem, A., *et al.,* (2017). Genotoxic and cytotoxic potential of whole plant extracts of Kalanchoe laciniata by Ames and MTT assay. *EXCLI J*. **16**: 593-

601.

Simioni, C., Zauli, G., Martelli, A.M., Vitale, M., *et al.,* (2018). Oxidative stress: role of physical exercise and antioxidant nutraceuticals in adulthood and aging. *Oncotarget.* **9** (24):17181-17198.

Srivastava, A., Singh, P. and Gupta, V.K. (2020) 'DFT studies on the electronic properties and reactivity of natural compounds', *Journal of Molecular Structure*, 1202, p. 127236.

Uddin, M.S., Al Mamun, A. and Rahman, M.M. (2021) 'Nrf2/Keap1 signaling pathway: A new perspective for neuroprotection', *Frontiers in Pharmacology*, 12, pp. 654–665.

Valko, M., Jomova, K., Rhodes, C.J., Kuca, K. and Musilek, K. (2016). Redox-and non-redox-metal-induced formation of free radicals and their role in human disease. *Arch. Toxicol*. **90** (1): 1–37.

Veber, D.F., Johnson, S.R., Cheng, H.Y., Smith, B.R., Ward, K.W. and Kopple, K.D. (2002) 'Molecular properties that influence the oral bioavailability of drug candidates', *Journal of Medicinal Chemistry*, 45(12), pp. 2615–2623.

Wadaan, M.A., Baabdad, A. and Khan, M.F. (2024). Assessment of antidiabetic, anti-inflammatory, antioxidant and anticancer activity competence of methanolic extracts of *Trianthema ortulacastrum*. *Environmental Research.* **242**: 117764.

Wang, L., Wu, Y. and Deng, Y. (2019) 'Accurate and reliable prediction of relative ligand binding potency using MM/GBSA', *Journal of Chemical Information and Modeling*, 59(7), pp. 3124–3137.

Wang, X., Liu, Z. and Zhang, J. (2020) 'Molecular docking and dynamics simulation studies of natural compounds targeting BCL-2', *Journal of Biomolecular Structure and Dynamics*, 38(14), pp. 4221–4233.

Xu, M., Jung, X., Hines, O.J., Eibl, G. and Chen, Y. (2018). Obesity and pancreatic cancer: overview of epidemiology and potential prevention by weight loss. Pancreas **47**(2): 158.

Yilmazer-Musa, M., *et al.,* 2012. Grape seed and tea extracts and catechin 3-gallates are potent inhibitors of α-amylase and 8924–8929.

Zellner, B.D.A., Dugo, P., Dugo, G. and Mondello, L. (2010). Analysis of essential oils. In handbook of essential oils: Science, Technology and Applications; Eds, Basser, K.H.C., Buchbauer, G; CRC Press, Taylor and Francis Group: London, UK.

Zhang, J., Huang, Z., Chen, W. and Chen, Y. (2008). Insulin resistance induced by high glucose and high insulin in HepG2 cells: a model for studying glucose metabolism and insulin signaling. *Biochemical and Biophysical Research Communications*, **372**(4), 816–821.

Zylla, D., Gilmore, G., Eklund, J., Richter, S. and Carlson, A. (2019). Impact of diabetes and hyperglycemia on health care utilization, infection risk, and survival in patients with cancer receiving glucocorticoids with chemotherapy. *J. Diabetes Complicat*. **33** (4): 335–339.